Electrochemistry Communications 124 (2021) 106920

Contents lists available at ScienceDirect

Electrochemistry Communications

journal homepage: www.elsevier.com/locate/elecom

MXene-functionalised 3D-printed electrodes for electrochemical capacitors

Edurne Redondo [a], Martin Pumera [a,b,c,d,*]

[a] Future Energy and Innovation Laboratory, Central European Institute of Technology, Brno University of Technology, Purkynova 123, Brno 61200, Czech Republic
[b] Department of Chemical and Biomolecular Engineering, Yonsei University, 50 Yonsei-ro, Seodaemun-gu, Seoul 03722, Republic of Korea
[c] Department of Chemistry and Biochemistry, Mendel University in Brno, Zemedelska 1, Brno 61300, Czech Republic
[d] Department of Medical Research, China Medical University Hospital, China Medical University, No. 91 Hsueh-Shih Road, Taichung, Taiwan

ARTICLE INFO

Keywords:
MXene
Ti_3C_2
3D printing
Functionalisation
Electrochemical capacitor

ABSTRACT

3D printing is a manufacturing technique that can be used to produce electrochemical capacitors with customised shapes and minimal material waste. However, the range of carbon-additive filaments currently commercially available is limited, resulting in 3D-printed electrodes with a poor capacitive performance due to their high thermoplastic content. Herein, a novel approach is presented for enhancing the electrochemical properties of 3D-printed electrodes, based on electrochemical activation of the electrodes followed by MXene functionalisation. Archetypal MXene, Ti_3C_2, has been used to modify the 3D-printed electrode surface; it has been demonstrated that it enhances the capacitance of the electrodes almost three-fold. These findings show a new route towards enhancing the performance of 3D-printed electrochemical capacitors and pave the way for further developments leading to other electrochemical applications.

1. Introduction

3D printing (or additive manufacturing) is a technology that has lately attracted great interest, as it permits rapid and easy prototyping and fabrication of customised components and objects [1]. The traditional manufacture of energy storage devices, such as supercapacitors, involves several time-consuming and costly processes. Examples of these processes include drying electrode coatings, electrolyte infilling, electrode calendering, electrode stamping and heat sealing [2]. These processes could be avoided if a continuous layer-by-layer 3D-printing process was used. Further benefits of this new manufacturing process include the maximum utilisation of materials with little wastage and the ability to construct more space-efficient energy-storage systems [3].

Unfortunately, the current selection of printable conductive inks or filaments is rather limited. The most promising for electrochemical capacitor applications is a conductive nanocarbon/polylactic acid (PLA)-based filament [4,5]. In its original state, this contains more than 90% thermoplastic PLA, which hinders the electrochemical activity of the nanocarbon but is currently necessary for effective 3D printing by fused filament fabrication (FFF) [6]. Nevertheless, this PLA can beremoved after printing using a variety of methods, e.g. thermal, electrochemical, solvent activations or polishing [7–12]. This results in an overall high nanocarbon content which greatly improves the electronic properties of the 3D-printed structure and enables its use as an electrode for electrochemical devices.

The materials used to fabricate 3D-printed electrodes are not always electrocatalytic or suitable for the intended application. Further modification of 3D-printed electrodes can be achieved via atomic layer deposition or electrodeposition [13–17]. However, electrodeposition or ALD is not possible for all materials due to the lack of available precursors [18]. One group of materials which cannot currently be electrodeposited or deposited by ALD are MXenes.

MXenes are 2D materials inspired by the study of graphene and transition metal dichalcogenides [19], which are composed of the carbides and nitrides of transition metals [20]. MXenes can be obtained by etching the A element (usually Al) from a MAX phase material, where M is an early transition metal and X is C and/or N. The result is a nanomaterial with a high surface area [21]. Ti_3C_2 is the most widely studied MXene. It has been found to have good applicability as an electrode material for electrochemical capacitors [22–24]; this is due to its

Abbreviations: PLA, polylactic acid; FFF, fused filament fabrication; 3DnCEs, 3D-printed nanocomposite carbon electrodes; Ti_3C_2@3DnCEs, MXene-unctionalised 3D-printed nanocarbon electrodes; PBS, phosphate buffer solution; SEM, scanning electron microscopy; XPS, X-ray photoelectron spectroscopy; CV, cyclic voltammetry; EIS, electrochemical impedance spectroscopy; GA, galvanostatic analysis; EDS, energy-dispersive X-ray spectroscopy.

* Corresponding author at: Future Energy and Innovation Laboratory, Central European Institute of Technology, Brno University of Technology, Purkynova 123, Brno 61200, Czech Republic.

E-mail address: pumera.group@gmail.com (M. Pumera).

https://doi.org/10.1016/j.elecom.2021.106920
Received 7 December 2020; Received in revised form 29 December 2020; Accepted 7 January 2021
Available online 19 January 2021

hydrophilicity, high electronic conductivity and also its ability to undergo redox capacitive processes at the Ti sites. The development of aqueous Ti_3C_2 inks without any additives has enabled its use in stamping, printing, painting and writing [25], and thus, the fabrication of flexible electrochemical capacitors and micro-supercapacitors [26–29], providing areal capacitance values of 5 mF cm^{-2}. With the addition of graphene oxide to the inks the capacitance has been increased to 2 F cm^{-2} [30]. Furthermore, owing to the ability of Ti_3C_2 to bond and to form composites with carbon materials [31,32], it is also a good candidate for the functionalisation of nanocarbon-based 3D-printed electrodes.

In this work we demonstrate for the first time that 3D-printed nanocarbon electrodes (3DnCEs) can be functionalised with Ti_3C_2 by a protocol that includes electrochemical activation of the electrodes followed by immersion of the electrodes in a MXene dispersion. Ti_3C_2 improves the performance of electrochemical capacitors using 3DnCEs, both as an additional active material ruled by a diffusion-limited storage process, and as a conductive additive to interconnect the graphene. Thus, MXene-functionalised 3D-printed nanocarbon electrodes (Ti_3C_2@3DnCEs) show enhanced capacitive behaviour.

2. Experimental section

2.1. 3D printing and functionalisation of the electrodes

3D-printed electrodes were produced by FFF using a commercially available Blackmagic conductive nanocarbon PLA filament (Graphene Supermarket, USA). The electrode shape resembled a circular lollipop on a stick; it consisted of an 11 mm diameter disc-shaped electrode with a 3 × 25 mm rectangular stick protruding from it. The thickness of the printed parts was 300 μm and the shape was designed with Fusion 360 software (Autodesk, USA) and sliced using PrusaSlicer software. The 3D-printed electrodes were produced with a Prusa I3 MK3 printer (Prusa Research, Czech Republic) with an Olsson Ruby ruby-tipped 0.4 mm nozzle (3DVerkstan, Sweden). Printing was done with a 215 °C nozzle temperature and a 60 °C bed temperature. The total mass of the 3D-printed electrodes was 49.5 mg and the mass of the circular part was 27.5 mg.

The electrodes were electrochemically activated by applying a constant potential of 2.5 V vs. Ag/AgCl for 1000 s in a phosphate buffer solution (PBS) at pH 7.2, using a Pt wire as the counter electrode. Then, the electrochemically activated 3D-printed electrodes were immersed in a vial containing 1.0 mg mL^{-1} MXene solution and stirred for 12 h. The MXene solution was prepared by diluting a Ti_3C_2 dispersion (Carbon-Ukraine, Ukraine) with deionised water and sonicating it for 30 min.

2.2. Materials characterisation

The surface of the electrodes was visualised by scanning electron microscopy (SEM) and energy-dispersive X-ray spectroscopy (EDS), using a LYRA3 instrument (Tescan Orsay Holding, Czech Republic) with an electron beam accelerating voltage of 5 kV. The atomic composition of the 3D-printed electrodes was analysed by X-ray photoelectron spectroscopy (XPS) using an AXIS Supra instrument (Kratos Analytical, Japan) with monochromatic Al Kα (1486.7 eV) excitation source, and the spectra were fitted using CasaXPS software. The crystallinity of the 3D-printed electrodes was analysed through Raman spectroscopy using an Alpha 300R instrument (Witec, Germany) with a 50× objective magnification, 5 mW laser power at 532 nm excitation wavelength and a CCD detector.

2.3. Electrochemical characterisation

Electrochemical measurements were performed using an Autolab PGSTAT204 potentiostat (Metrohm, Switzerland). All the measurements were done in a three-electrode configuration using a beaker cell and immersing only the circular part of the electrode in the electrolyte. Characterisation against a redox probe was carried out by performing cyclic voltammetry (CV) experiments at a scan rate of 25 mV s^{-1} in a solution of 1 mM $[Fe(CN)_6]^{4-/3-}$ in 0.1 M KCl, using Pt wire as the counter electrode and a Ag/AgCl reference electrode. The corresponding electrochemical impedance spectroscopy (EIS) experiments were conducted at frequencies from 100 kHz to 100 mHz at a voltage of 0.2 V vs. Ag/AgCl and an amplitude of 10 mV. The 3D-printed electrodes for supercapacitors were characterised using CV, galvanostatic (GA) charge–discharge cycling and EIS experiments in a 2 M sulphuric acid (H_2SO_4) aqueous solution, with a Pt wire counter electrode and a Ag/AgCl reference electrode. EIS measurements were carried out by applying a low sinusoidal amplitude alternating voltage of 10 mV at frequencies from 100 kHz to 10 mHz.

3. Results and discussion

The fabrication of the free-standing MXene-modified 3D-printed nanocarbon electrodes (Ti_3C_2@3DnCE) is schematically illustrated in Scheme 1a. The first step is 3D printing of the electrodes by FFF, followed by electrochemical activation and then functionalisation with a MXene solution. The resulting Ti_3C_2@3DnCE shows a great increase in capacitance (Scheme 1b) without any apparent signs of degradation or shape alteration (Fig. S1).

The SEM image (Fig. 1a) shows that the surface of 3DnCE has been modified with MXene sheets. The Ti_3C_2@3DnCE surface is mainly composed of PLA covering fibrous nanocarbon. This otherwise amorphous surface has been disrupted by the formation of grooves, in which the lamellar-structured MXene particles have been embedded. Energy-dispersive X-ray spectroscopy (EDS), used to study the type of elements present, confirms that the lamellar particles identified as MXene are composed of C, O and Ti (Fig. 1b). F was also detected, although in smaller quantities. Since MXenes are commonly etched using hydrofluoric acid they typically end up with fluorinated functional groups. Further XPS analysis was carried out to investigate the nature of the Ti_3C_2@3DnCE. The survey spectrum (Fig. 1c) supports the results from EDS, corroborating the presence of C, O and Ti elements at atomic concentrations of 68.4, 31.5 and 0.1%, respectively. Moreover, core level XPS scans in the C 1s, O 1s and Ti 2p regions were conducted to elucidate the nature of the bonding environment. The C 1s core level (Fig. S2a) shows three main peaks associated with the composition of the PLA, i.e. C═O, C–O and C–C, which appear at 289, 287 and 285 eV, respectively. Another main peak, assigned to the C═C bonds of the nanocarbon, is also present at 284 eV. More importantly, a small peak is observed at 282 eV, originating from C-Ti bonds, and sustaining the argument that MXene is present in the Ti_3C_2@3DnCE. The O 1s core level (Fig. S2b) shows only the two peaks corresponding to C═O and C–O from the PLA. Furthermore, the Ti 2p core level (Fig. S2c) clearly demonstrates that MXene is present in the Ti_3C_2@3DnCE, as Ti–C and Ti–O duplets can be identified at 456 and 459 eV, respectively. The Raman spectrum (Fig. 1d) provides some complementary information regarding the crystallinity or otherwise of the Ti_3C_2@3DnCE. The main peaks observed originate from the nanocarbon; these are the D and G peaks at 1349 and 1581 cm^{-1}, respectively, and a 2D peak at 2689 cm^{-1} [33]. The fact that the ratio of intensity between D and G bands (I_D/I_G) is ~0.8 demonstrates that the carbonaceous structure is defect rich, due to the amorphous nature of the PLA present. Due to the low concentration of MXene on the Ti_3C_2@3DnCE no other characteristic peak for this compound could be found in the Raman spectrum.

Additionally, the electrochemical activity of the Ti_3C_2@3DnCE was tested with respect to the $[Fe(CN)_6]^{4-/3-}$ redox probe. The CVs (Fig. 2a) show that, after MXene functionalisation, the current at the Ti_3C_2@3DnCE electrodes increased. Despite the Ti_3C_2@3DnCE being unable to provide the oxidation and reduction peaks of the $[Fe(CN)_6]^{4-/3-}$ redox couple, due to the absence of surface oxides on the nanocarbon [34], it is noteworthy that the capacitance of Ti_3C_2@3DnCE has

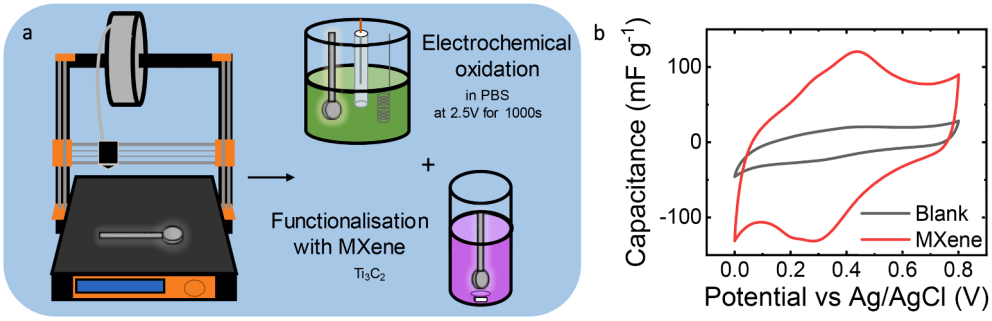

Scheme 1. Preparation of the Ti_3C_2@3DnCE. (a) Illustration of the fabrication of 3D-printed nanocarbon electrodes using FFF and their subsequent modification by means of electrochemical activation and MXene functionalisation. (b) Enhanced capacitance of the Ti_3C_2@3DnCE in 2 M H_2SO_4.

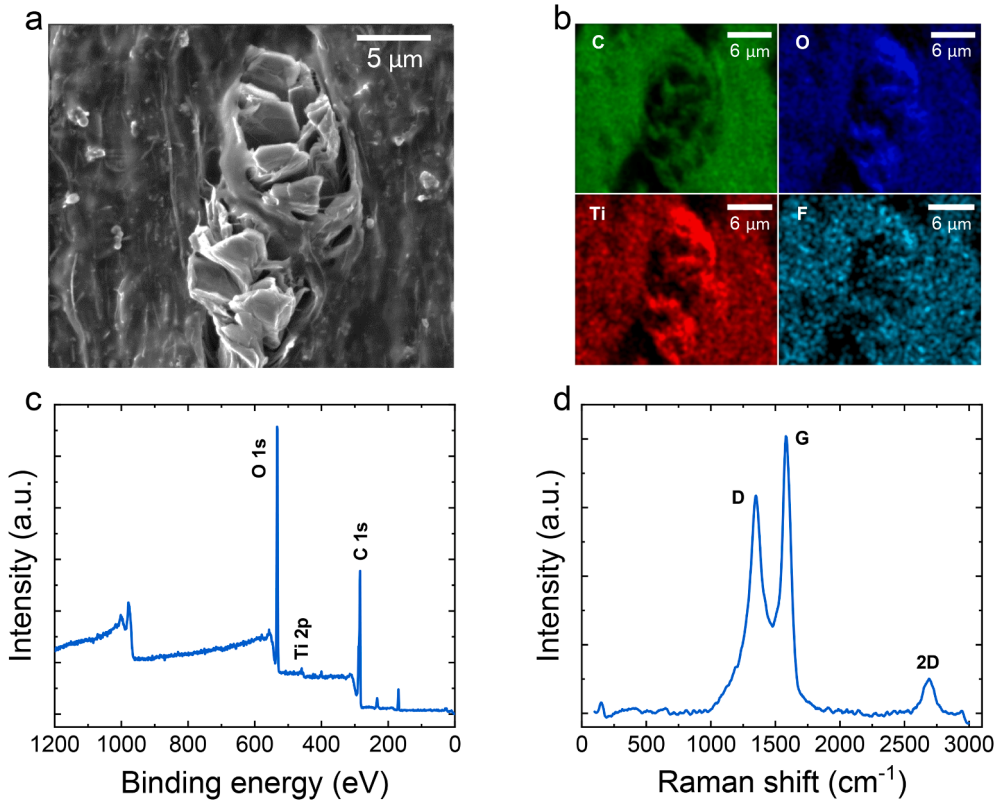

Fig. 1. (a) SEM image and (b) EDS analysis of the Ti_3C_2@3DnCE, showing the modification of 3DnCE with Ti_3C_2. (c) XPS of the Ti_3C_2@3DnCE, revealing the presence of Ti 2p. (d) Raman spectrum of the Ti_3C_2@3DnCE, mainly showing the nanocarbon bands.

increased with respect to the 3DnCE. This result suggests that the electroactive surface area has been increased by adding MXene to the 3DnCE. The Nyquist plots of the bare 3DnCE and Ti_3C_2@3DnCE (Fig. 2b and c) show a semi-straight line at low frequencies which is related to the diffusion processes. The EIS data was fitted using the Randles circuit shown in Fig. S3 and the corresponding data is summarised in Table S1. The values of the resistances, both the solution resistance and the charge-transfer resistance, decrease when Ti_3C_2@3DnCE is used. This indicates that the presence of MXene on the surface of the 3DnCE facilitates the electron transfer and diffusion-limiting processes. Furthermore, the double-layer capacitance and Warburg impedance both increase after the addition of MXene.

Owing to the remarkable increase in capacitance displayed by the Ti_3C_2@3DnCE, further studies, including CVs, GA and EIS, were conducted in 2 M H_2SO_4 electrolyte in order to characterise this electrode as a potential candidate for electrochemical capacitor applications. Interestingly, as shown in the CVs (Fig. 3a), the Ti_3C_2@3DnCE does not exhibit the typical rectangular shape characteristic of supercapacitors, as opposed to the 3DnCE (Fig. S4a). Instead, Ti_3C_2@3DnCE displays two broad oxidation and reduction peaks, suggesting that this electrode not only has a surface capacitive mechanism, but also a diffusion-controlled one. In order to determine the capacitive contribution of Ti_3C_2@3DnCE, the current response was related to the scan rate using Eq. (1):

$$i/v^{1/2} = k_1 v^{1/2} + k_2 \quad (1)$$

where i is the current, v is the scan rate and k_1 and k_2 are the factors relating the surface capacitive effect and the diffusion-controlled process, respectively. Using the CVs recorded at different scan rates, $i/v^{1/2}$ was plotted against $v^{1/2}$ and k_1 and k_2 extracted from the slope and the intercept of this plot, respectively [35]. Thus, the capacitive contribution of the Ti_3C_2@3DnCE was determined to be 34%. Fig. 3b shows that the peaks present in the curve of the total current are absent in the curve of the capacitive contribution. This indicates that they are part of a diffusion-controlled process in the bulk of the material. Fig. S4b depicts

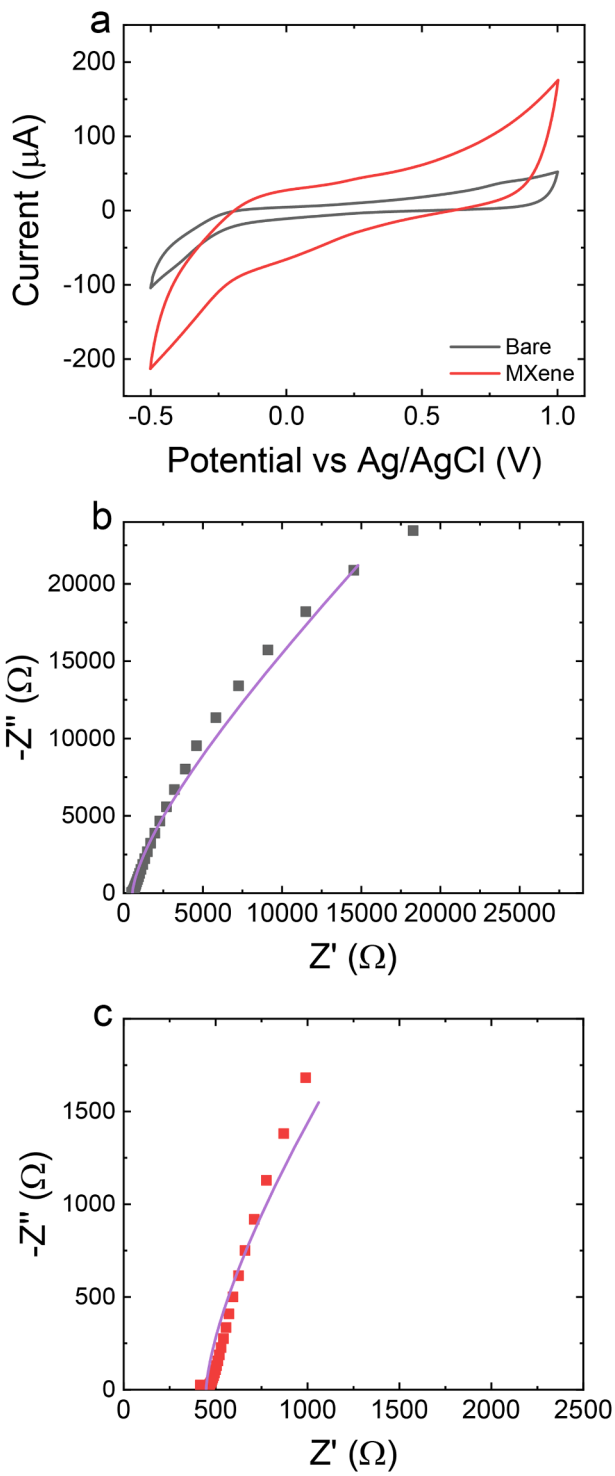

Fig. 2. Electrochemical activity of the Ti_3C_2@3DnCE in $[Fe(CN)_6]^{4-/3-}$ in 0.1 M KCl electrolyte. (a) CVs of Ti_3C_2@3DnCE at 25 mV s^{-1}; EIS of (b) 3DnCE and (c) Ti_3C_2@3DnCE at 0.2 V from 100 kHz to 100 mHz.

the comparison between the total and capacitive contribution to the current of the bare 3DnCE. Its capacitive part is impressively low, only 6%. This might be because of the very resistive nature of the PLA, which is the major component of the bare 3DnCE. This mechanistic difference clearly demonstrates the positive effect of adding MXene to the 3DnCE, as this increases the capacitive part of the current as well as providing extra capacity through redox peaks. Therefore, Ti_3C_2 may be acting both as an additive material interconnecting the nanocarbon and as an active material through the additional pseudocapacitance.

Figs. 3c and S4c show the GA charge–discharge profiles of the Ti_3C_2@3DnCE and bare 3DnCE, respectively. The Ti_3C_2@3DnCE displays quasi-triangular-shaped charge–discharge profiles, with a small 'plateau' at ~0.4 V. This plateau is linked to the peaks observed in the CVs, corresponding to the redox processes occurring at the Ti sites of the MXene. The coulombic efficiency of the Ti_3C_2@3DnCE at 10 μA is 66%, demonstrating the incomplete reversibility of the reaction. Figs. 3d and S4d show the rate capability of the Ti_3C_2@3DnCE and bare 3DnCE. Both electrodes show a big capacitance loss for current densities higher than 50 μA. The Ti_3C_2@3DnCE retains 74% of the capacitance before that sharp loss while the 3DnCE retains 86%. However, the gravimetric and areal capacitance of the Ti_3C_2@3DnCE are still 2.6 times higher than those of the 3DnCE, with values of 194 mF g^{-1} and 7 mF cm^{-2}, respectively, at 10 μA. It should be noted that these capacitance values are also more than double those reported for additive-free MXene inks [25].

Figs. 3e and S4e show the Nyquist plots of the Ti_3C_2@3DnCE and bare 3DnCE, respectively. These plots form a large semicircle towards low frequencies. The lack of a vertical increase in the imaginary part of the impedance indicates that the Ti3C2@3DnCE does not achieve typical capacitive storage [36]. The EIS data was fitted using the equivalent circuits shown in Fig. S5 for the Ti_3C_2@3DnCE and in Fig. S3 for 3DnCE, and the obtained values are summarised in Table S2. Both resistances, the solution resistance and the charge transfer resistance, have smaller values for the Ti_3C_2@3DnCE than for the 3DnCE, which confirms improved electrochemical behaviour after MXene functionalisation. The value of the capacitance increases for the Ti_3C_2@3DnCE.

The frequency behaviour of the Ti_3C_2@3DnCE and bare 3DnCE was studied using derived Bode plots (Figs. 3f and S4f, respectively), based on the modelling of the capacitance in the real (C_{real}) and the imaginary ($C_{imaginary}$) parts [37], calculated from the EIS using Eqs. (2) and (3):

$$C_{real} = -Z_{imaginary}/\left(\omega|Z|^2\right) \quad (2)$$

$$C_{imaginary} = Z_{real}/\left(\omega|Z|^2\right) \quad (3)$$

where $Z_{imaginary}$ and Z_{real} are the imaginary and real impedance, ω is the angular frequency ($\omega = 2\pi f$), f is the frequency and Z is the impedance. From the real part, Ti_3C_2@3DnCE has a purely resistive behaviour at high frequencies and a purely capacitive one at low frequencies, with the maximum capacitance reached at a value of 57 mF g^{-1}, as all the surface has been filled with electrolyte ions. Half of the total capacitance has a value of 31 mF g^{-1} and is obtained at 0.20 Hz, corresponding to the capacitance value for a phase angle of −45° [38]. The relaxation time (τ_0) was calculated from $\tau_0 = 1/f_0$, using the maximum imaginary capacitance, yielding a value of 5 s. This value is related to the electrolyte accessibility to the electrode surface and is higher for the Ti_3C_2@3DnCE than for the bare 3DnCE (3 s), suggesting that electrolyte penetration depends upon functionalisation of the electrode surface. A cyclability study of Ti_3C_2@3DnCE was carried out at 1 μA (Fig. S6). Ti_3C_2@3DnCE shows a good capacitance retention of 92% after 700 cycles.

4. Conclusions

In this work 3D-printed nanocarbon electrodes underwent surface modification using Ti_3C_2. This was achieved through electrochemical activation of the 3DnCE material and subsequent Ti_3C_2 functionalisation. Comprehensive characterisation of Ti_3C_2@3DnCEs has been performed using SEM, EDS, XPS and Raman spectroscopy to determine the resulting composition and material structure. Ti_3C_2@3DnCEs were then been tested as electrochemical capacitors and found to give superior capacitance compared to bare 3DnCEs. This is due to the ability of MXene material to undergo diffusion-controlled redox processes alongside surface capacitive processes. Improvements also arose from the

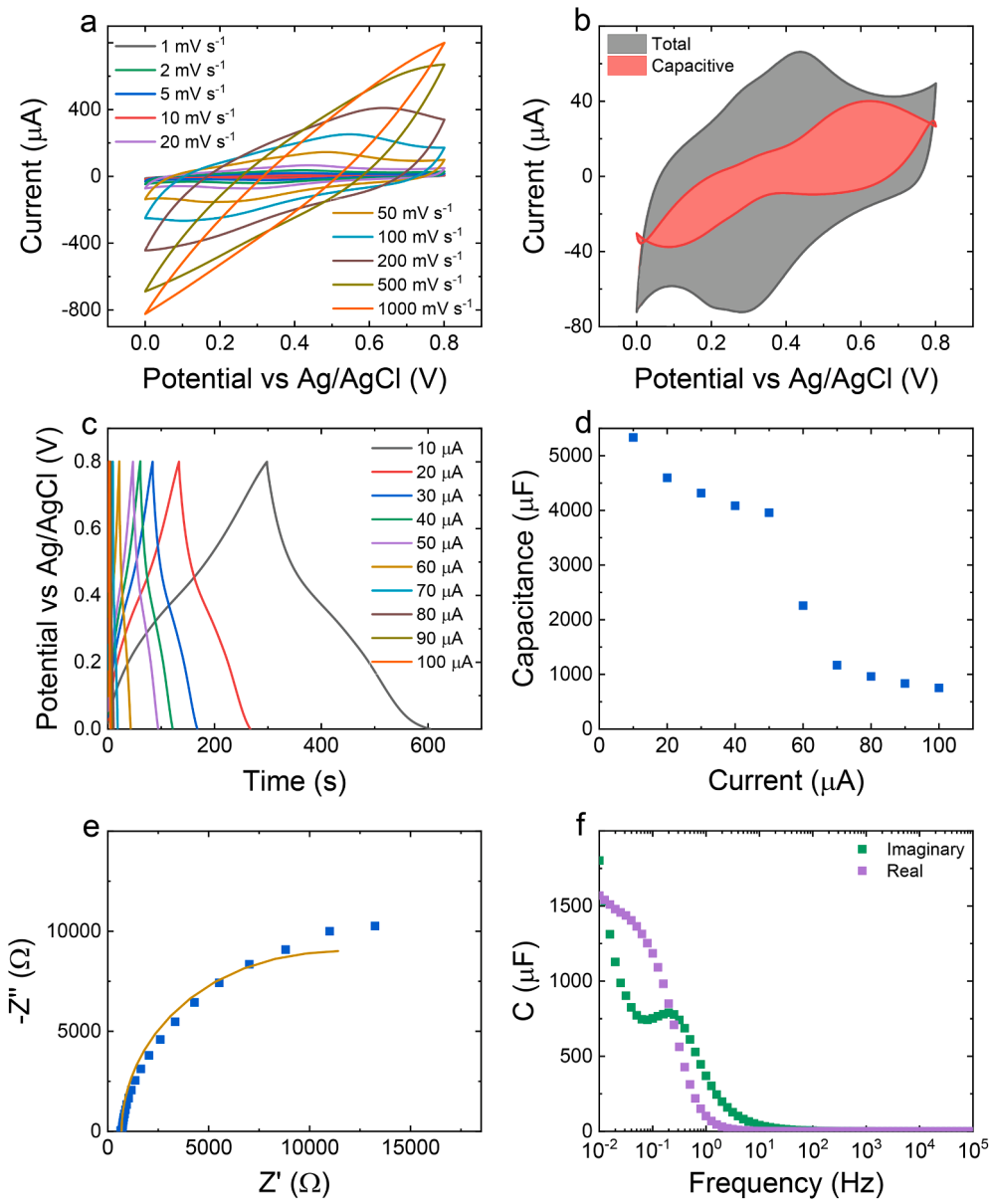

Fig. 3. Electrochemical characterisation of Ti_3C_2@3DnCE for electrochemical capacitors in 2 M H_2SO_4 using a three-electrode cell. (a) CVs at different scan rates and (b) analysis of the capacitive current contribution of Ti_3C_2@3DnCE. (c) Galvanostatic charge–discharge cycles at different currents and (d) the derived rate capability. (e) Nyquist plot showing the measured data (indicated by dots) and the fitted data (continuous line) and (f) the derived Bode plot of the Ti_3C_2@3DnCE.

improved interconnection of graphene by the MXene material. Hence, it is possible to obtain advanced 3D-printed electrochemical capacitors through MXene functionalisation. This work opens up new opportunities for the functionalisation of 3DnCE for use in electrochemical applications.

Declaration of Competing Interest

The authors declare that they have no known competing financial interests or personal relationships that could have appeared to influence the work reported in this paper.

Acknowledgements

M.P. acknowledges the financial support of the Grant Agency of the Czech Republic by the GACR EXPRO 19-26896X project. E.R. acknowledges CzechNanoLab Research Infrastructure supported by LM2018110 MEYS CR 2020–2022. The authors would like to thank Dr. Richard Fields for English correction.

Appendix A. Supplementary data

Photograph of the 3DnCE and Ti_3C_2@3DnCE; XPS of the Ti_3C_2@3DnCE; equivalent circuit used for the impedance data fitting in $[Fe(CN)_6]^{4-/3-}$; values of the parameters obtained after fitting the EIS; electrochemical characterisation of 3DnCE for electrochemical capacitors in 2M H_2SO_4 using a three electrode cell; equivalent circuit used for the impedance data fitting of the Ti_3C_2@3DnCE for electrochemical capacitor; values of the parameters obtained after fitting the EIS as supercapacitors; cyclability study of the Ti_3C_2@3DnCE. Supplementary data to this article can be found online at https://doi.org/10.1016/j.elecom.2021.106920.

References

[1] M.P. Browne, E. Redondo, M. Pumera, 3D printing for electrochemical energy applications, Chem. Rev. 120 (2020) 2783–2810, https://doi.org/10.1021/acs.chemrev.9b00783.

[2] M. Schmitt, R. Diehm, P. Scharfer, W. Schabel, An experimental and analytical study on intermittent slot die coating of viscoelastic battery slurries, J. Coat. Technol. Res. 12 (5) (2015) 927–938, https://doi.org/10.1007/s11998-015-9717-9.

[3] J. Muñoz, M. Pumera, 3D-printed biosensors for electrochemical and optical applications, TrAC, Trends Anal. Chem. 128 (2020) 115933, https://doi.org/10.1016/j.trac.2020.115933.

[4] C.W. Foster, M.P. Down, Y. Zhang, X. Ji, S.J. Rowley-Neale, G.C. Smith, P.J. Kelly, C.E. Banks, 3D printed graphene based energy storage devices, Sci. Rep. 7 (2017) 42233, https://doi.org/10.1038/srep42233.

[5] P.F. Flowers, C. Reyes, S. Ye, M.J. Kim, B.J. Wiley, 3D printing electronic components and circuits with conductive thermoplastic filament, Addit. Manuf. 18 (2017) 156–163, https://doi.org/10.1016/j.addma.2017.10.002.

[6] E. Redondo, S. Ng, J. Munoz, M. Pumera, Tailoring capacitance of 3D-printed graphene electrodes by carbonisation temperature, Nanoscale 12 (2020) 19673–19680, https://doi.org/10.1039/D0NR04864J.

[7] F. Novotny, V. Urbanova, J. Plutnar, M. Pumera, Preserving fine structure details and dramatically enhancing electron transfer rates in graphene 3D-printed electrodes via thermal annealing: toward nitroaromatic explosives sensing, ACS Appl. Mater. Interfaces 11 (2019) 35371–35375, https://doi.org/10.1021/acsami.9b06683.

[8] M.P. Browne, F. Novotný, Z. Sofer, M. Pumera, 3D printed graphene electrodes' electrochemical activation, ACS Appl. Mater. Interfaces 10 (46) (2018) 40294–40301, https://doi.org/10.1021/acsami.8b14701.

[9] R. Gusmão, M.P. Browne, Z. Sofer, M. Pumera, The capacitance and electron transfer of 3D-printed graphene electrodes are dramatically influenced by the type of solvent used for pre-treatment, Electrochem. Commun. 102 (2019) 83–88, https://doi.org/10.1016/j.elecom.2019.04.004.

[10] C.L. Manzanares Palenzuela, F. Novotny, P. Krupicka, Z. Sofer, M. Pumera, 3D-printed graphene/polylactic acid electrodes promise high sensitivity in electroanalysis, Anal. Chem. 90 (9) (2018) 5753–5757, https://doi.org/10.1021/acs.analchem.8b00083.

[11] C. Kalinke, N.V. Neumsteir, G.O. Aparecido, T.V.B. Ferraz, P.L. Dos Santos, B. C. Janegitz, J.A. Bonacin, Comparison of activation processes for 3D printed PLA-graphene electrodes: electrochemical properties and application for sensing of dopamine, Analyst 145 (4) (2020) 1207–1218, https://doi.org/10.1039/C9AN01926J.

[12] R.M. Cardoso, P.R.L. Silva, A.P. Lima, D.P. Rocha, T.C. Oliveira, T.M. do Prado, E. L. Fava, O. Fatibello-Filho, E.M. Richter, R.A.A. Muñoz, 3D-printed graphene/polylactic acid electrode for bioanalysis: biosensing of glucose and simultaneous determination of uric acid and nitrite in biological fluids, Sens. Actuators, B 307 (2020), 127621, https://doi.org/10.1016/j.snb.2019.127621.

[13] C.Y. Foo, H.N. Lim, M.A. Mahdi, M.H. Wahid, N.M. Huang, Three-dimensional printed electrode and its novel applications in electronic devices, Sci. Rep. 8 (1) (2018) 7399, https://doi.org/10.1038/s41598-018-25861-3.

[14] K.P.A. Kumar, K. Ghosh, O. Alduhaish, M. Pumera, Metal-plated 3D-printed electrode for electrochemical detection of carbohydrates, Electrochem. Commun. 120 (2020), 106827, https://doi.org/10.1016/j.elecom.2020.106827.

[15] S. Ng, C. Iffelsberger, Z. Sofer, M. Pumera, Tunable room-temperature synthesis of ReS_2 bicatalyst on 3D- and 2D-printed electrodes for photo- and electrochemical energy applications, Adv. Funct. Mater. 30 (19) (2020) 1910193, https://doi.org/10.1002/adfm.201910193.

[16] M.P. Browne, J. Plutnar, A.M. Pourrahimi, Z. Sofer, M. Pumera, Atomic layer deposition as a general method turns any 3D-printed electrode into a desired catalyst: case study in photoelectrochemisty, Adv. Energy Mater. 9 (26) (2019) 1900994, https://doi.org/10.1002/aenm.201900994.

[17] C. Iffelsberger, S. Ng, M. Pumera, Catalyst coating of 3D printed structures via electrochemical deposition: case of the transition metal chalcogenide MoS_x for hydrogen evolution reaction, Appl. Mater. Today 20 (2020), 100654, https://doi.org/10.1016/j.apmt.2020.100654.

[18] F. Dvorak, R. Zazpe, M. Krbal, H. Sopha, J. Prikryl, S. Ng, L. Hromadko, F. Bures, J. M. Macak, One-dimensional anodic TiO_2 nanotubes coated by atomic layer deposition: towards advanced applications, Appl. Mater. Today 14 (2019) 1–20, https://doi.org/10.1016/j.apmt.2018.11.005.

[19] C.C. Mayorga-Martinez, A. Ambrosi, A.Y.S. Eng, Z. Sofer, M. Pumera, Transition metal dichalcogenides (MoS_2, $MoSe_2$, WS_2 and WSe_2) exfoliation technique has strong influence upon their capacitance, Electrochem. Commun. 56 (2015) 24–28, https://doi.org/10.1016/j.elecom.2015.03.017.

[20] K. Li, M. Liang, H. Wang, X. Wang, Y. Huang, J. Coelho, S. Pinilla, Y. Zhang, F. Qi, V. Nicolosi, Y. Xu, 3D MXene architectures for efficient energy storage and conversion, Adv. Funct. Mater. 20 (47) (2020) 2000842, https://doi.org/10.1002/adfm.202000842.

[21] M. Naguib, M. Kurtoglu, V. Presser, J. Lu, J. Niu, M. Heon, L. Hultman, Y. Gogotsi, M.W. Barsoum, Two-dimensional nanocrystals produced by exfoliation of Ti_3AlC_2, Adv. Mater. 23 (37) (2011) 4248–4253, https://doi.org/10.1002/adma.201102306.

[22] V. Bayram, M. Ghidiu, J.J. Byun, S.D. Rawson, P. Yang, S.A. McDonald, M. Lindley, S. Fairclough, S.J. Haigh, P.J. Withers, M.W. Barsoum, I.A. Kinloch, S. Barg, MXene tunable lamellae architectures for supercapacitor electrodes, ACS Appl. Energy Mater. 3 (1) (2019) 411–422, https://doi.org/10.1021/acsaem.9b01654.

[23] A.M. Navarro-Suárez, K.L. Van Aken, T. Mathis, T. Makaryan, J. Yan, J. Carretero-González, T. Rojo, Y. Gogotsi, Development of asymmetric supercapacitors with titanium carbide-reduced graphene oxide couples as electrodes, Electrochim. Acta 259 (2018) 752–761, https://doi.org/10.1016/j.electacta.2017.10.125.

[24] C. Couly, M. Alhabeb, K.L. Van Aken, N. Kurra, L. Gomes, A.M. Navarro-Suárez, B. Anasori, H.N. Alshareef, Y. Gogotsi, Asymmetric flexible MXene-reduced graphene oxide micro-supercapacitor, Adv. Electron. Mater. 4 (1) (2018) 1700339, https://doi.org/10.1002/aelm.201700339.

[25] E. Quain, T.S. Mathis, N. Kurra, K. Maleski, K.L. Van Aken, M. Alhabeb, H. N. Alshareef, Y. Gogotsi, Direct writing of additive-free MXene-in-water ink for electronics and energy storage, Adv. Mater. Technol. 4 (1) (2019) 1800256, https://doi.org/10.1002/admt.201800256.

[26] C.J. Zhang, M.P. Kremer, A. Seral-Ascaso, S.-H. Park, N. McEvoy, B. Anasori, Y. Gogotsi, V. Nicolosi, Stamping of flexible, coplanar micro-supercapacitors using MXene inks, Adv. Funct. Mater. 28 (9) (2018) 1705506, https://doi.org/10.1002/adfm.201705506.

[27] L. Yu, Z. Fan, Y. Shao, Z. Tian, J. Sun, Z. Liu, Versatile N-doped MXene ink for printed electrochemical energy storage application, Adv. Energy Mater. 9 (34) (2019) 1901839, https://doi.org/10.1002/aenm.201901839.

[28] C.J. Zhang, L. McKeon, M.P. Kremer, S.H. Park, O. Ronan, A. Seral-Ascaso, S. Barwich, C.O. Coileain, N. McEvoy, H.C. Nerl, B. Anasori, J.N. Coleman, Y. Gogotsi, V. Nicolosi, Additive-free MXene inks and direct printing of micro-supercapacitors, Nat. Commun. 10 (1) (2019) 1795, https://doi.org/10.1038/s41467-019-09398-1.

[29] J. Orangi, F. Hamade, V.A. Davis, M. Beidaghi, 3D printing of additive-free 2D $Ti_3C_2T_x$ (MXene) ink for fabrication of micro-supercapacitors with ultra-high energy densities, ACS Nano 14 (1) (2020) 640–650, https://doi.org/10.1021/acsnano.9b07325.

[30] W. Yang, J. Yang, J.J. Byun, F.P. Moissinac, J. Xu, S.J. Haigh, M. Domingos, M. A. Bissett, R.A.W. Dryfe, S. Barg, 3D printing of freestanding MXene architectures for current-collector-free supercapacitors, Adv. Mater. 31 (37) (2019), e1902725, https://doi.org/10.1002/adma.201902725.

[31] L. Yu, L. Hu, B. Anasori, Y.-T. Liu, Q. Zhu, P. Zhang, Y. Gogotsi, B. Xu, MXene-bonded activated carbon as a flexible electrode for high-performance supercapacitors, ACS Energy Lett. 3 (7) (2018) 1597–1603, https://doi.org/10.1021/acsenergylett.8b00718.

[32] T. Zhou, C. Wu, Y. Wang, A.P. Tomsia, M. Li, E. Saiz, S. Fang, R.H. Baughman, L. Jiang, Q. Cheng, Super-tough MXene-functionalized graphene sheets, Nat. Commun. 11 (1) (2020) 2077, https://doi.org/10.1038/s41467-020-15991-6.

[33] A.C. Ferrari, D.M. Basko, Raman spectroscopy as a versatile tool for studying the properties of graphene, Nat. Nanotechnol. 8 (4) (2013) 235–246, https://doi.org/10.1038/nnano.2013.46.

[34] R.L. McCreery, Advanced carbon electrode materials for molecular electrochemistry, Chem. Rev. 108 (2008) 2646–2687, https://doi.org/10.1021/cr068076m.

[35] A.M. Navarro-Suárez, N. Casado, J. Carretero-González, D. Mecerreyes, T. Rojo, Full-cell quinone/hydroquinone supercapacitors based on partially reduced graphite oxide and lignin/PEDOT electrodes, J. Mater. Chem. A 5 (15) (2017) 7137–7143, https://doi.org/10.1039/C7TA00527J.

[36] W.-Y. Tsai, R. Lin, S. Murali, L. Li Zhang, J.K. McDonough, R.S. Ruoff, P.-L. Taberna, Y. Gogotsi, P. Simon, Outstanding performance of activated graphene based supercapacitors in ionic liquid electrolyte from −50 to 80 °C, Nano Energy 2 (3) (2013) 403–411, https://doi.org/10.1016/j.nanoen.2012.11.006.

[37] P.L. Taberna, P. Simon, J.F. Fauvarque, Electrochemical characteristics and impedance spectroscopy studies of carbon-carbon supercapacitors, J. Electrochem. Soc. 150 (2003) A292–A300, https://doi.org/10.1149/1.1543948.

[38] W.-Y. Tsai, P.-C. Gao, B. Daffos, P.-L. Taberna, C.R. Perez, Y. Gogotsi, F. Favier, P. Simon, Ordered mesoporous silicon carbide-derived carbon for high-power supercapacitors, Electrochem. Commun. 34 (2013) 109–112, https://doi.org/10.1016/j.elecom.2013.05.031.